Int. J. Electrochem. Sci., 15 **(2020)** 9204 – 9222, doi: 10.20964/2020.09.102

International Journal of
ELECTROCHEMICAL
SCIENCE
www.electrochemsci.org

Investigation of Inhibition of Stress Corrosion Cracking of Welded Ti-6Al-4V Alloy using Electrochemical Noise

Yan Liu[1,*], *Jicai Feng*[2], *Shuping Tan*[1], *Yi Cheng*[1], *Jin Hu*[3,*]

[1] State Key Laboratory of Efficient and Clean Coal-Fired Utility Boilers, Harbin Boiler Company Limited, Harbin 150046, China
[2] State Key Laboratory of Advanced Welding and Joining, Harbin Institute of Technology, Harbin 150001, China
[3] School of Materials Science and Engineering, Harbin Institute of Technology, Harbin 150001, China
[*]E-mail: liuyan_research@yeah.net, hujin@hit.edu.cn

Received: 2 May 2020 / *Accepted:* 20 June 2020 / *Published:* 10 August 2020

In this study, the effect of residual stress on the stress corrosion cracking behavior of welded Ti-6Al-4V alloy was investigated by means of electrochemical noise. The residual stress is effectively relaxed by local rapid induction heating, and the higher heat treatment temperature leads to lower residual stress. The residual stress has a significant effect on the mechanical properties and sensitivity of stress corrosion cracking under the slow strain rate tensile test, which respectively increases and decreases continuously with the gradual relaxation of residual stress. The results indicate that a sample with lower residual stress shows higher corrosion resistance and later occurrence time of localized corrosion during the slow strain rate tensile test. The relaxation of residual stress significantly inhibits the stress corrosion cracking process.

Keywords: Electrochemical noise; Residual stress; welded Ti-6Al-4V alloy; Stress corrosion cracking

1. INTRODUCTION

Titanium alloy is a new type of engineering material with high specific strength, low thermal conductivity, good damping capacity, and excellent heat resistance and corrosion resistance, and it has been widely employed in the aerospace, automobile and chemical industries as steel [1,2]. At present, the application range of titanium alloys is gradually expanding and the usage of this material in various fields is continuously increasing [3-5]. Welding technology has become the important processing method in the manufacturing field of titanium alloy [6-9]. For welded titanium alloy, the uneven temperature field and the change of microstructure during the welding process will inevitably lead to welding residual stress, and the existence of residual stress will have a great influence on many properties

[10-13]. Stress corrosion cracking may occur in titanium alloy during the application process, and the residual stress is the main factor affecting stress corrosion cracking behavior [14-17]. The residual stress may induce high sensitivity of stress corrosion cracking of welded titanium alloy in specific corrosion mediums [18-22]. Therefore, it is necessary to adjust the residual stress of welded titanium alloy to inhibit the stress corrosion cracking and enhance the safety and stability. Unfortunately, there has been little research conducted in the abovementioned area.

After years of continuous development, electrochemical noise has become an effective method for studying the electrochemical corrosion process; it can monitor the key information in the electrode reaction process and has been widely used in the corrosion research of various metal materials [23-27]. At present, the stress corrosion cracking behavior of steel and nickel alloy has been studied by the combination of electrochemical noise and the slow strain rate tensile test, but there has been almost no research conducted regarding titanium alloy and its welded joints [28-31]. In this study, local rapid induction heating was employed to adjust the residual stress of welded Ti-6Al-4V alloy, and the control of residual stress for inhibiting stress corrosion cracking of welded Ti-6Al-4V was investigated by describing the electrochemical noise during the process of the slow strain rate tensile test.

2. EXPERIMENTAL PROCEDURE

2.1 Material

Commercial annealed Ti-6Al-4V alloy sheets with a size of 240 mm×50 mm×1 mm were used in this study, and the chemical composition is shown in Table 1.

Table 1. Chemical compositions (wt.%) of commercial annealed Ti-6Al-4V alloy sheets.

Element	Ti	Al	V	Fe	Si	C	O	H	N
Content	Balance	5.9	4.0	0.08	0.005	0.02	0.1	0.002	0.03

2.2 Welding process

In this study, Ti-6Al-4V alloy sheets were welded via a Rofin-DC030 pulse laser welding system. The faying and joining surfaces of all Ti-6Al-4V alloy sheets were mechanically brushed, acid pickled in hydrofluoric acid solution and then cleaned by acetone to remove any contaminants and surface oxides prior to the clamping and welding. The laser beam was focused on the top surface of the workpiece. Because Ti-6Al-4V alloy was highly reactive with ambient gases at high temperature, the fusion zone and heat-affected zone of the welded joint was shielded using ultrahigh-purity argon gas until they were cooled below the reactivity temperature during the welding process. The welding parameters are listed in Table 2.

Table 2. Laser welding process parameters of commercial annealed welded Ti-6Al-4V alloy sheets via a Rofin-DC030 pulse laser welding system.

Parameters	Power (W)	Frequency (Hz)	Welding speed (m/min)	Argon pressure (MPa)
Value	800	35	1	0.12

2.3 Local rapid induction heating

This study applied reciprocating local rapid induction heating to adjust the residual stress of welded Ti-6Al-4V alloy. The local rapid induction heating system was composed of a 60-kW/25-kHz solid-state induction power supply and induction coil, and the induction coil was used to scan the workpiece. The temperature of induction heating was 500 ℃, 600 ℃ and 700 ℃, respectively, which was measured and controlled by turning the induction power supply off and on as needed based on an infrared thermometer focused on the surface of the workpiece. The induction coil was located directly above the workpiece, the heating width was 20 mm, and the reciprocating speed was 120 mm/min with 15 reciprocating instances. The power supply was turned off at the end of induction heating, and the workpieces were placed in air and cooled to room temperature. Figure 1 exhibits the schematic diagram of the induction heating process, and the moving direction of the workpiece is displayed by the black arrow.

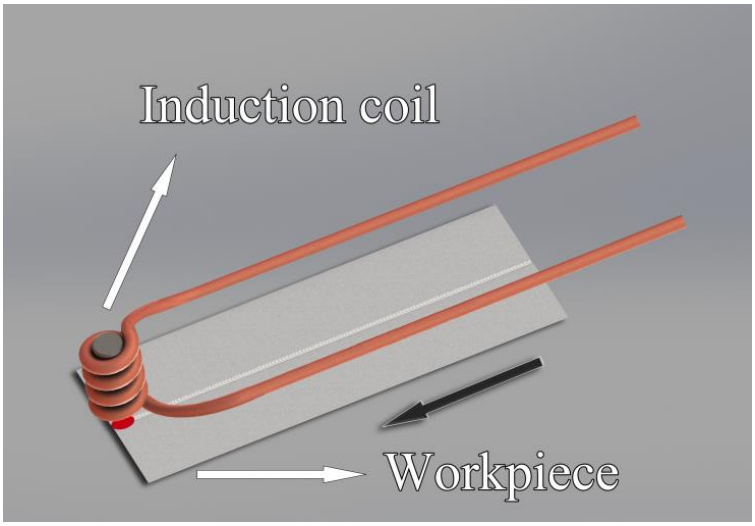

Figure 1. Schematic diagram of local rapid induction heating for commercial annealed welded Ti-6Al-4V alloy sheets via a Rofin-DC030 pulse laser welding system.

2.4 Residual stress measurement

A Philips X-Pert diffractometer with a parallel Cu Kα radiation source was used to analyze the residual stress distribution in welded Ti-6Al-4V alloy through the traditional $\sin^2\psi$ method. The step of

the 2θ angle was 0.05°, and the scan speed per step was 1 s. The diffraction angle 2θ required to calculate the residual stress was 70°-72°, and $\sin^2\psi$ was set at 0, 0.05, 0.1, 0.15, 0.2, 0.25 and 0.3 for each measurement point. The peak search result and 2θ-$\sin^2\psi$ were subsequently recorded, and the slope of $\Delta(2\theta)/\Delta(\sin^2\psi)$ was determined by the linear equation least square method. In the measurement, the working voltage was 40 kV, and the working current was 40 mA.

2.5 Slow strain rate tensile test

Stress corrosion cracking of welded Ti-6Al-4V alloy was investigated through a LETRY-WDL-1000 slow strain rate tensile testing machine with a constant strain rate of 3×10^{-7}/s; this accelerated test provides reliable information on stress corrosion cracking susceptibility and has been widely used. A polytetrafluoroethylene cell with end caps was used to form a reaction chamber. The dimensions of the tensile sample are shown in Figure 2. The sample only exposed the weld seam to the corrosive medium, and the remaining area was sealed with silicone rubber. The tensile samples were uniaxially loaded in the slow strain rate tensile machine at room temperature, and the test continued until the samples fractured completely. For comparison, the samples were also measured in air under the same strain rate at room temperature. The elongation and tensile strength were achieved for each sample after the slow strain rate tensile test, and this approach helped to quantify the change in the mechanical properties of the samples. The corrosion medium used for the tests was 0.1 M lithium chloride-methanol solution prepared from analytical-grade chemical reagents. Each test was repeated three times, and the presented result is the average value of these tests. It was noticed that there was no apparent discrepancy among the test results, and the results were thus considered to be reliable and reproducible.

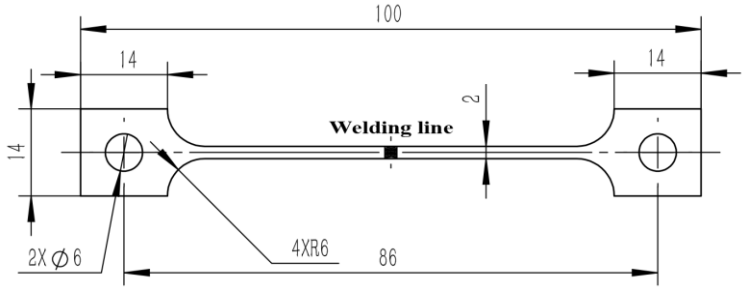

Figure 2. Dimensions of tensile samples of commercial annealed welded Ti-6Al-4V alloy sheets via a Rofin-DC030 pulse laser welding system tested under the slow strain rate tensile test with a strain rate of 3×10^{-7}/s in 0.1 M lithium chloride-methanol solution, mm.

2.6 Electrochemical noise measurement

In this study, a Gamry Reference 3000 electrochemical workstation was employed to measure the electrochemical noise of welded Ti-6Al-4V alloy under the slow strain rate tensile test. It is difficult to achieve the same state between the two tensile samples in the process of electrochemical noise measurement, so the improved electrochemical noise measuring technology "Electrochemical Emission Spectroscopy" was applied by using the reference electrode as the silver/silver chloride/methanol

electrode, the working electrode as the tensile sample, and the counter electrode as the platinum microcathode [32-37]. Different from the traditional electrochemical noise measurement, there was only one working electrode in the three-electrode test system during the modified measurement, and the other working electrode was replaced by a microcathode with a sufficiently small area. Therefore, the working electrode was still in a self-corrosion state after being coupled with the microcathode, and the corrosion behavior of the working electrode eventually remained unchanged. During the process of electrochemical noise measurement, the current noise signal was simultaneously monitored as a function of testing time between the tensile sample and the counter electrode using a zero-resistance ammeter. No bias voltage was applied to the tensile sample, and the measurement acquisition was performed over a period of 512 s with a sampling frequency of 10 Hz, which corresponded to a sampling time of 0.1 s. Measurements were stopped until the tensile samples fractured completely during the slow strain rate tensile test. The direct current component in the original noise signal was removed from the measured data before time-domain analysis and frequency-domain analysis. Each test was carried out with three replicates to ensure the measurement repeatability.

3. RESULTS AND DISCUSSION

3.1 Residual stress in welded Ti-6Al-4V alloy

Figure 3 shows the residual stress distribution in welded Ti-6Al-4V alloy before and after induction heating. For the nontreated sample, there is a tensile stress zone located between the welding centerline and the position located approximately 20 mm away from the weld seam center. The peak value of the tensile stress appears at the center of the weld seam and reaches 317 MPa, indicating that a high level of residual stress has been introduced during the welding process. As the distance from the weld seam center gradually increases, the residual stress value decreases rapidly and is close to 0 MPa at the edge of the tensile stress zone. Because the internal stress has the function of self-equilibrium, the compressive stress appears in the area outside of the tensile stress zone, and the peak value of the compressive stress reaches -73 MPa, which appears at the position located approximately 30 mm away from the weld seam center. Subsequently, the residual stress fluctuates and changes into tensile stress with a value of 24 MPa again at the position located approximately 40 mm away from the weld seam center.

After the induction heating, the distribution trend of residual stress on the side of the weld seam is largely the same. The residual stress at the center of the weld seam is significantly relaxed and decreases rapidly, and the stress at the position located away from the weld seam center also decreases by varying degrees. The effect of induction heating on stress relaxation is clearly related to the heating temperature, and a higher temperature caused a lower value of residual stress. When the induction heating temperature is 700C, the tensile stress at the weld seam center is reduced from 317 MPa to 47 MPa, which is 85.3% lower than that of the nontreated sample. This result indicates that the residual stress of the welded Ti-6Al-4V alloy has been effectively relieved through the induction heating treatment. Related research used an electron beam to perform local heat treatment on welded Ti-6Al-4V

alloy and obtained a conclusion similar to that of this study [38]. It was found that tensile stress with a peak value of 553 MPa existed near the center of the weld seam, and the stress reduced rapidly with increasing distance from the weld seam center. The stress value at the position located approximately 5 mm away from the weld seam center was 0 MPa, and compressive stress with a peak value of -86 MPa appeared at the position located 12 mm away from the center of the weld seam. The value of residual stress at the weld seam center was reduced to 131 MPa after electron beam treatment and was 76% lower than that of the nontreated sample, which indicated that the residual stress was effectively released [38].

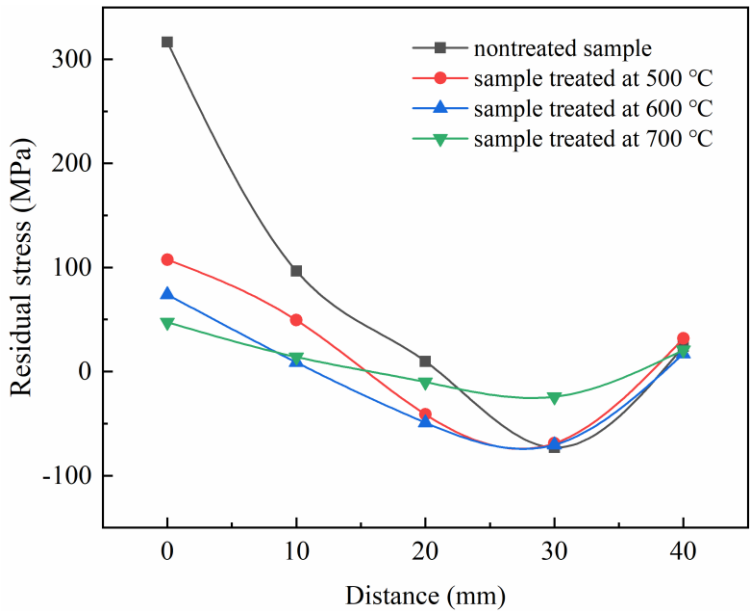

Figure 3. Residual stress distribution in commercial annealed welded Ti-6Al-4V alloy sheets via a Rofin-DC030 pulse laser welding system before and after local rapid induction heating with different heat treatment temperatures.

3.2 Stress corrosion cracking of welded Ti-6Al-4V alloy

The slow strain rate tensile test was applied to welded Ti-6Al-4V alloy to investigate the stress corrosion cracking in this study [39-44]. Figure 4 displays the stress-strain curves obtained from the slow strain rate tensile test of samples before and after induction heating in air and 0.1 M lithium chloride-methanol solution. It can be seen that the curves obtained in air are almost the same no matter how the processing parameters of induction heating are changed or whether the sample is subjected to induction heating or not, which shows that the mechanical properties are hardly affected. The mechanical properties of samples tested in 0.1 M lithium chloride-methanol solution are significantly lower than those of samples tested in air, indicating that obvious sensitivities of stress corrosion cracking exist in the welded joint. Related studies have reported similar results for Ti-6Al-4V alloy tested under the slow strain rate tensile test in air and 0.6% hydrochloric acid-methanol solution, and the elongation of a sample tested in 0.6% hydrochloric acid-methanol solution showed a significant decrease compared with that of a sample tested in air [45,46].

The residual stress relaxation through induction heating greatly enhances the mechanical properties obtained in 0.1 M lithium chloride-methanol solution, which increased with increasing induction heating temperature. By comparing the mechanical properties of a nontreated sample and a sample treated at 700 ℃, it is found that the tensile strength and elongation increased by 77.8% and 91.7%, respectively.

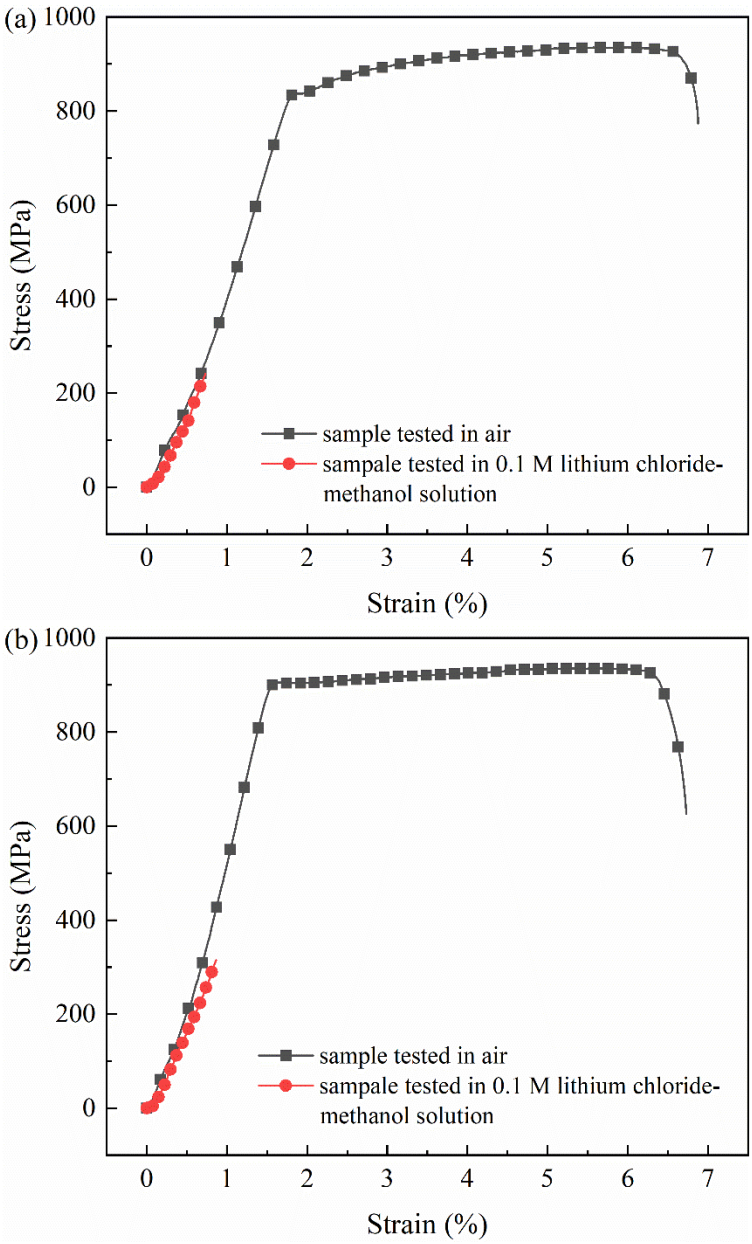

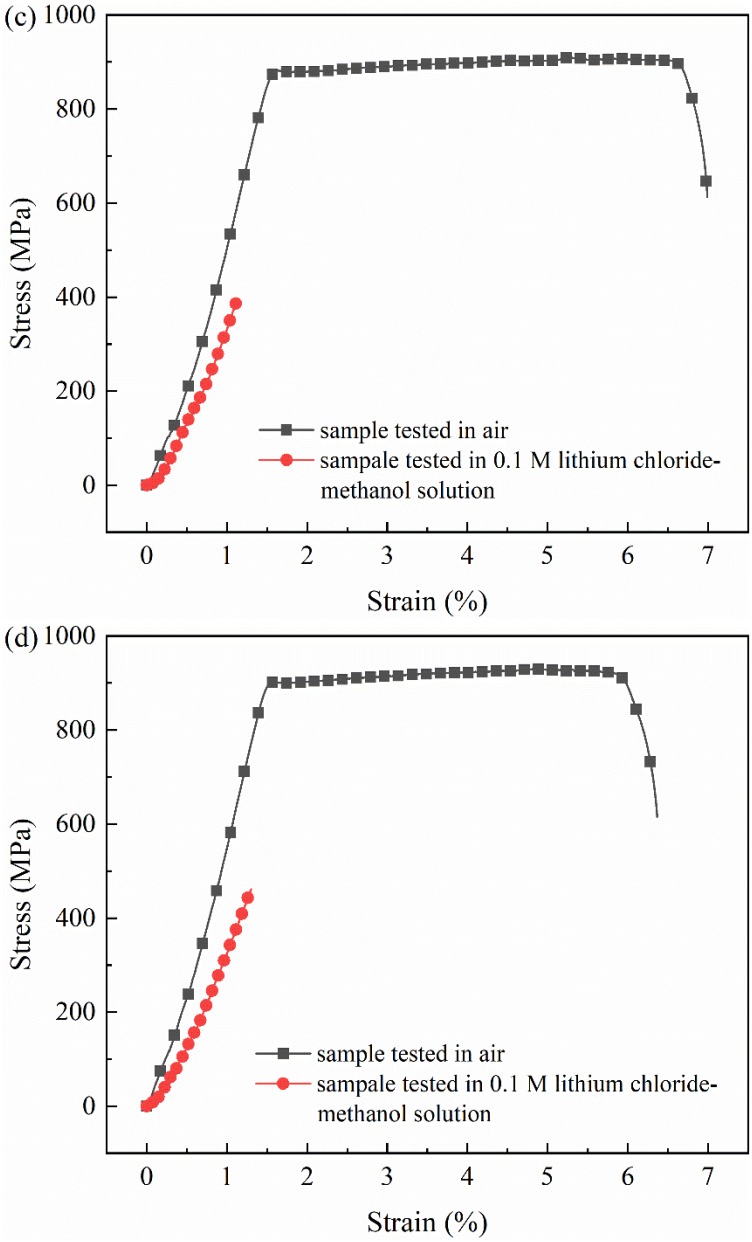

Figure 4. Stress-strain curves obtained from the slow strain rate tensile test with a strain rate of 3×10^{-7}/s of commercial annealed welded Ti-6Al-4V alloy sheets via a Rofin-DC030 pulse laser welding system before and after local rapid induction heating in air and 0.1 M lithium chloride-methanol solution: (a) nontreated sample, (b) sample treated at 500 ℃, (c) sample treated at 600 ℃, and (d) sample treated at 700 ℃.

This study also analyzed the stress corrosion cracking sensitivity of welded Ti-6Al-4V alloy by evaluating the sensitivity index which is mainly characterized by the relative difference between the mechanical properties of the samples tested in an inert medium and corrosion medium [47,48]. The calculation formulas of the sensitivity index are shown as follow:

$$I_\sigma\ (\%) = \frac{\sigma_{air} - \sigma_{sol}}{\sigma_{air}} \times 100 \quad (1)$$

$$I_{\varepsilon}\,(\%) = \frac{\varepsilon_{air} - \varepsilon_{sol}}{\varepsilon_{air}} \times 100 \quad (2)$$

where I_{σ} and I_{ε} represent the sensitivity index of strength and plasticity, σ_{air} and σ_{sol} represent the tensile strength obtained from samples tested in air and 0.1 M lithium chloride-methanol solution, ε_{air} and ε_{sol} represent the elongation obtained from samples tested in air and 0.1 M lithium chloride-methanol solution [38,39]. The mechanical properties and stress corrosion cracking sensitivities obtained from the slow strain rate tensile test of samples before and after induction heating in air and 0.1 M lithium chloride-methanol solution are shown in Table 3. It can be seen that the sensitivity index of strength and plasticity are greatly reduced by residual stress relaxation through induction heating, and a higher induction heating temperature causes a lower sensitivity index. Clearly, the stress corrosion cracking of welded Ti-6Al-4V alloy has been effectively inhibited by adjusting the residual stress. Similar results were also obtained by related studies, which indicated that the plastic sensitivity indexes of Ti-6Al-4V alloy tested in 0.6% hydrochloric acid-methanol solution containing hydrochloric acid were 52.1% and 92.5% under the slow strain rate tensile test [49,50].

Table 3. Mechanical properties and stress corrosion cracking sensitivities obtained from the slow strain rate tensile test with a strain rate of 3×10^{-7}/s of commercial annealed welded Ti-6Al-4V alloy sheets via a Rofin-DC030 pulse laser welding system before and after local rapid induction heating in air and 0.1 M lithium chloride-methanol solution.

Sample	Condition	Strength (MPa)	Strength sensitivity I_{σ} (%)	Elongation (%)	Strain sensitivity I_{ε} (%)
Nontreated	Air	936	74.25	6.88	89.39
Nontreated	0.1 M lithium chloride-methanol solution	241		0.73	
Treated at 500 °C	Air	936	66.35	6.73	87.61
Treated at 500 °C	0.1 M lithium chloride-methanol solution	315		0.86	
Treated at 600 °C	Air	909	56.55	6.99	83.83
Treated at 600 °C	0.1 M lithium chloride-methanol solution	395		1.13	
Treated at 700 °C	Air	930	50.32	6.37	80.48
Treated at 700 °C	0.1 M lithium chloride-methanol solution	462		1.30	

3.3 Removal of the direct current component in the electrochemical noise signal

The original electrochemical noise signal must be processed by removing the direct current component before analyzing the noise signal. Related studies have proved that the polynomial fitting method is highly effective for removing the direct current component in the signal [51]. Taking the current noise signal as an example, the polynomial fitting method mainly follows the following relationship when removing the direct current component:

$$I = I_0 + a_0 + a_1 t + a_2 t^2 + a_3 t^3 + \cdots + a_{\mathrm{n}} t^{\mathrm{n}} \quad (3)$$

where I represents the original current noise signal and I_0 represents the real current noise signal. In this study, the original electrochemical noise signal was processed by the quintic polynomial fitting method to remove the direct current component. At the same time, the required real signal can be retained to the greatest extent, and the effective information in the real signal cannot be weakened or even eliminated [52].

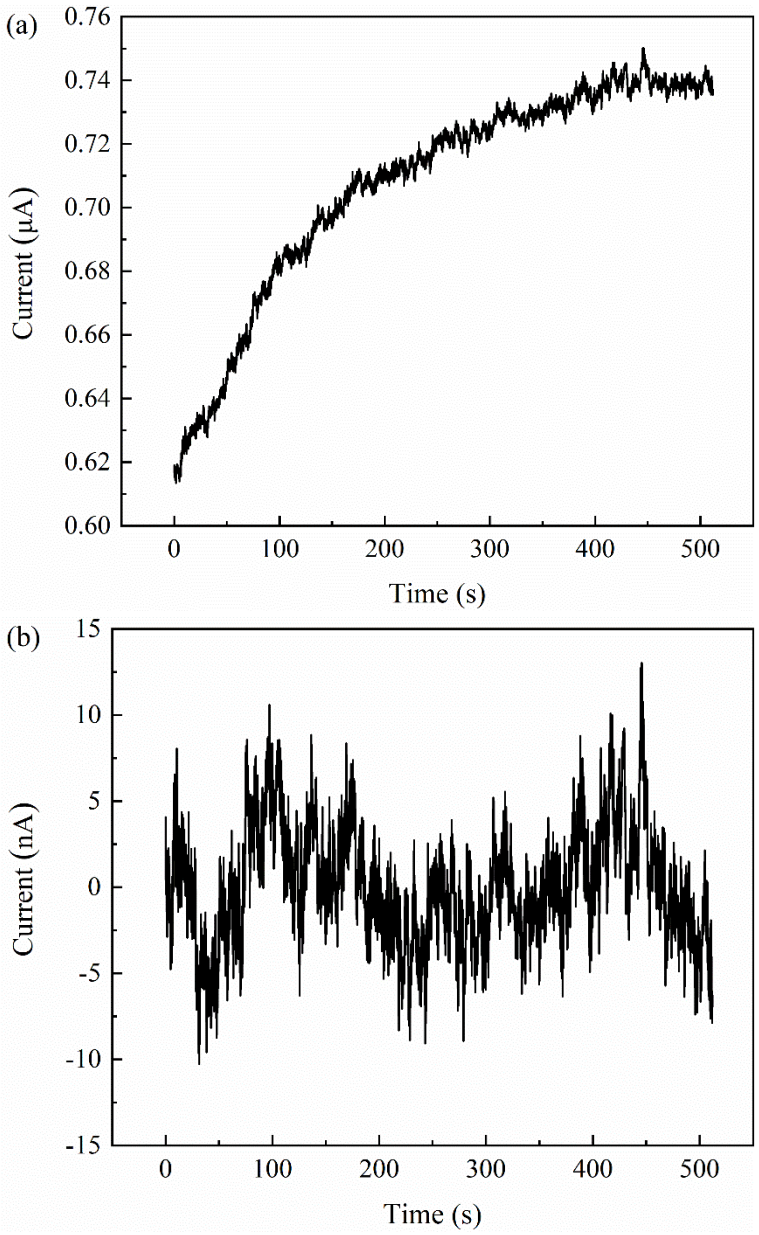

Figure 5. Current noise signal of the electrochemical noise measurement of commercial annealed welded Ti-6Al-4V alloy sheets via a Rofin-DC030 pulse laser welding system obtained from an unstressed immersion test in 0.1 M lithium chloride-methanol solution before and after removing the direct current component by the quintic polynomial fitting method: (a) original noise signal before removing the direct current component and (b) real noise signal after removing the direct current component.

To describe the effect of polynomial fitting on the removal of the direct current component, Figure 5 exhibits the current noise signal of Ti-6Al-4V alloy obtained from the immersion test before and after removing the direct current component. It is clear that the original noise signal distribution obviously changes after removing the direct current component, and the treated current noise signal fluctuates around the zero point, which indicates that the removal of the direct current component in the signal through the quintic polynomial fitting method is reasonable [51,52].

3.4 Time-domain analysis of the electrochemical noise signal

According to the above results in this study, the nontreated sample and the sample treated at 700 ℃ were selected for electrochemical noise analysis. At this time, there was a great difference in the residual stresses between the two samples, and it can effectively investigate the effect of residual stress on the stress corrosion cracking behavior.

The electrochemical noise resistance R_n, skewness coefficient S_k and kurtosis coefficient K_u have typically been used as the main parameters for time-domain analysis of the electrochemical noise signal [27,32]. The electrochemical noise resistance R_n is defined as the ratio of the standard deviation of the potential noise to the standard deviation of the current noise [53]. Taking the current noise signal as an example, the standard deviation is shown through the following formula:

$$S = \sqrt{\frac{1}{n-1}\sum_{i=1}^{n}\left(x_i - \frac{1}{n}\sum_{i=1}^{n}x_i\right)^2} \tag{4}$$

where x_i represents the measured transient value of the current noise signal and n represents the number of sampling points [54]. R_n has typically been used to describe the corrosion resistance of a material in a corrosion medium. Lower R_n represents worse corrosion resistance, a faster corrosion rate and a more serious corrosion process, while higher R_n means better corrosion resistance, a slower corrosion rate and a milder corrosion process [27,32,53-56].

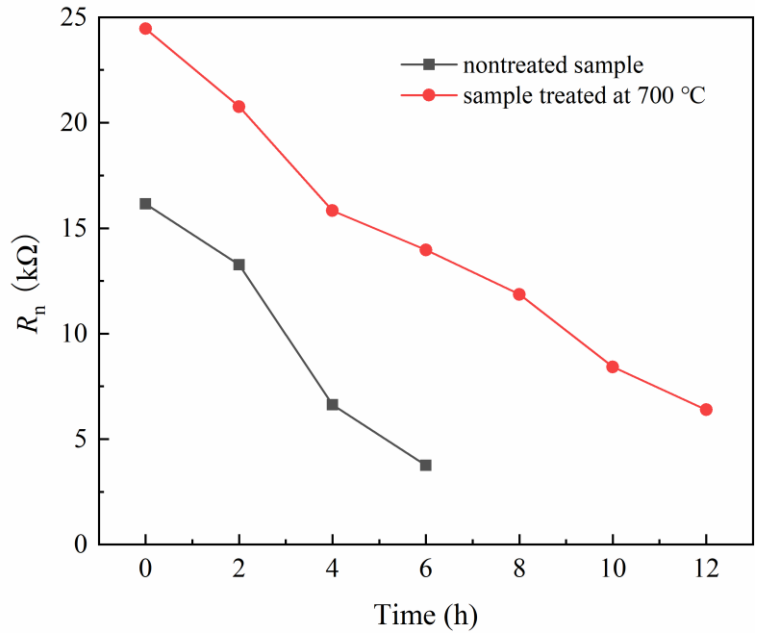

Figure 6. Electrochemical noise resistance R_n of the electrochemical noise measurement of commercial annealed welded Ti-6Al-4V alloy sheets via a Rofin-DC030 pulse laser welding system before and after local rapid induction heating with different time points obtained from the slow strain rate tensile test with a strain rate of 3×10^{-7}/s in 0.1 M lithium chloride-methanol solution.

The electrochemical noise resistance R_n of welded Ti-6Al-4V alloy before and after induction heating obtained from the slow strain rate tensile test is shown in Figure 6. It can be clearly seen that the noise resistance of the nontreated sample is relatively low with the highest value of approximately 17 kΩ during the slow strain rate tensile test. The noise resistance of the sample has been significantly improved after induction heating compared to that of the nontreated sample, and the highest value is approximately 25 kΩ at this time. The above results show that the relaxation of residual stress can effectively improve the corrosion resistance in the process of stress corrosion cracking. In addition, the noise resistances of the samples decrease gradually during the slow strain rate tensile test, which indicates that the applied load continuously reduces the corrosion resistances of the samples [57-59].

The skewness coefficient S_k and kurtosis coefficient K_u, which represent the high-order statistical parameters to measure the degree of deviation from symmetry and steepness of the electrochemical noise signal distribution, were also used in the aspect of time-domain analysis [60]. Taking the current noise signal as an example, the mathematical definition is shown via the following formula:

$$S_k = \frac{1}{(n-1)S^3}\sum_{i=1}^{n}(x_i - \bar{x})^3 \quad (5)$$

$$K_u = \frac{1}{(n-1)S^4}\sum_{i=1}^{n}(x_i - \bar{x})^4 \quad (6)$$

where S represents the standard deviation of the current noise signal, x_i represents the measured transient value of the current noise signal, $\bar{x}$ represents the average value of the current noise signal, and n represents the number of sampling points. Related studies have shown that a greater difference between

the S_k value and 0 or that between the K_u value and 3 always means a faster corrosion rate and worse corrosion resistance of the material [61].

Figure 7 displays the skewness coefficient S_k and kurtosis coefficient K_u of the current noise signal of welded Ti-6Al-4V alloy before and after induction heating obtained from the slow strain rate tensile test, and the absolute differences between the S_k value and 0 and between K_u and 3 are also shown together in the figure. It can be seen that the absolute difference of S_k and K_u of all samples shows the same change trend, which gradually increases during the slow strain rate tensile test. The absolute difference of S_k and K_u of the sample treated at 700 ℃ is obviously lower than that of the nontreated sample. The results show that the corrosion resistance of all samples during the slow strain rate tensile test gradually decreases and that the residual stress relaxation through induction heating significantly improves the corrosion resistance of the sample, which are completely consistent with the results obtained from electrochemical noise resistance analysis.

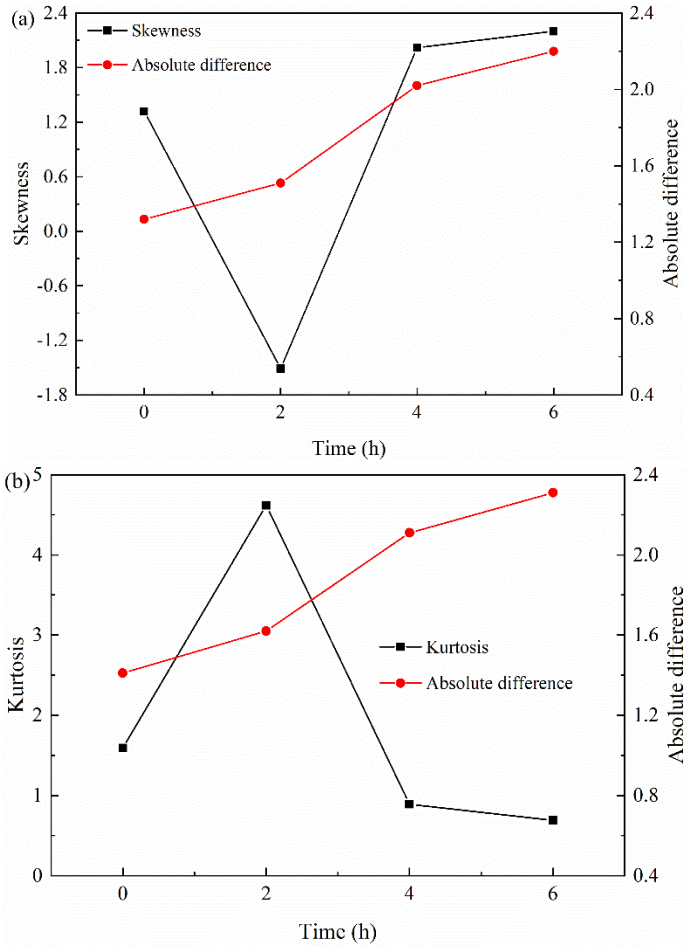

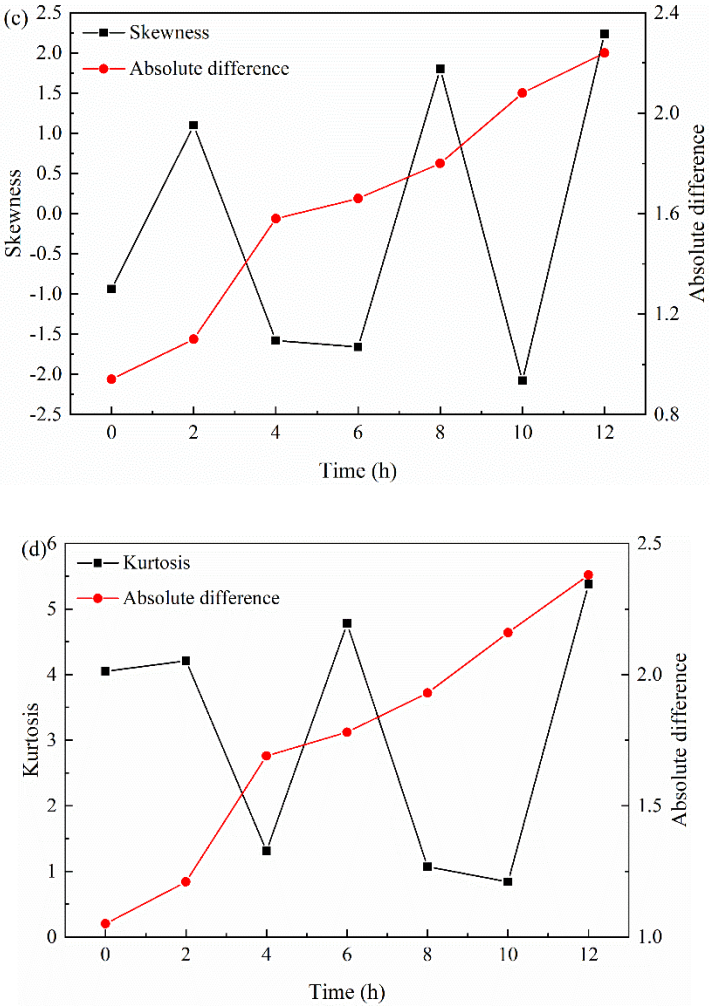

Figure 7. Skewness coefficient S_k and kurtosis coefficient K_u (absolute differences between the S_k value and 0 and between K_u and 3) of the current noise signal of the electrochemical noise measurement of commercial annealed welded Ti-6Al-4V alloy sheets via a Rofin-DC030 pulse laser welding system before and after local rapid induction heating with different time points obtained from the slow strain rate tensile test with a strain rate of 3×10^{-7}/s in 0.1 M lithium chloride-methanol solution: (a) S_k and its absolute difference of a nontreated sample, (b) K_u and its absolute difference of a nontreated sample, (c) S_k and its absolute difference of a sample treated at 700 ℃, and (d) K_u and its absolute difference of a sample treated at 700 ℃.

3.5 Frequency-domain analysis of the electrochemical noise signal

In general, it is difficult to fully characterize the corrosion process and its essential characteristics by analyzing the electrochemical noise signal in only the time-domain [32,55]. More useful information can be obtained by converting the noise signal from the time-domain to the frequency-domain for analysis [56,62-64]. The power spectral density (PSD) can be obtained after the noise signal is converted to the frequency-domain [65]. The slope is an important characterization parameter of frequency-domain analysis, which can be obtained by linear fitting of the PSD curve [66,67]. The information related to the electrode reaction process can be obtained by characterizing the slope, such as the corrosion type and corrosion tendency of the electrode [68,69]. Taking the current noise signal as an example, Figure 8

exhibits the PSD curve of the current noise signal of welded Ti-6Al-4V alloy before and after induction heating obtained from the slow strain rate tensile test.

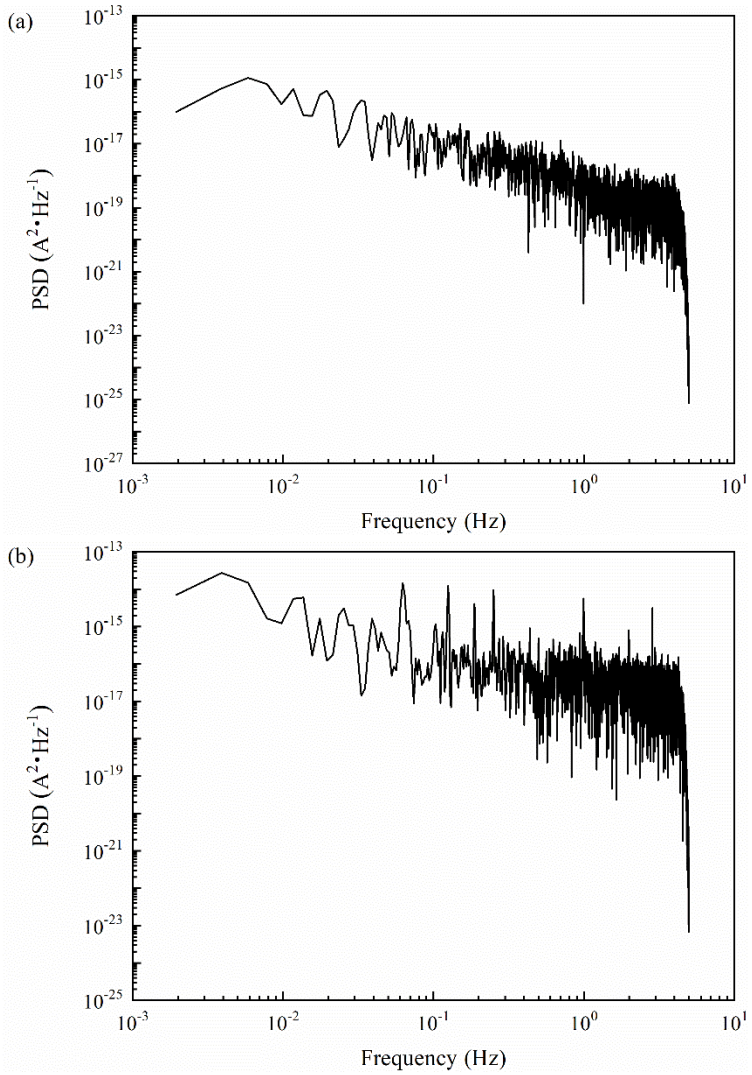

Figure 8. Power spectral density of the current noise signal of the electrochemical noise measurement of commercial annealed welded Ti-6Al-4V alloy sheets via a Rofin-DC030 pulse laser welding system before and after local rapid induction heating obtained from the initial stage of the slow strain rate tensile test with a strain rate of 3×10^{-7}/s in 0.1 M lithium chloride-methanol solution: (a) power spectral density of a nontreated sample and (b) power spectral density of a sample treated at 700 ℃.

The PSD curve slope of the current noise signal of welded Ti-6Al-4V alloy before and after induction heating obtained from the slow strain rate tensile test is shown in Figure 9. It can be seen that the slope of the nontreated sample tested at 0-4 h is lower than -20 dB/dec and higher than -20 dB/dec when the slow strain rate tensile test lasted for 6 h. However, the slope of the sample tested at 0-8 h is lower than -20 dB/dec after induction heating at 700 ℃, which is higher than -20 dB/dec when the sample was tested for 10-12 h.

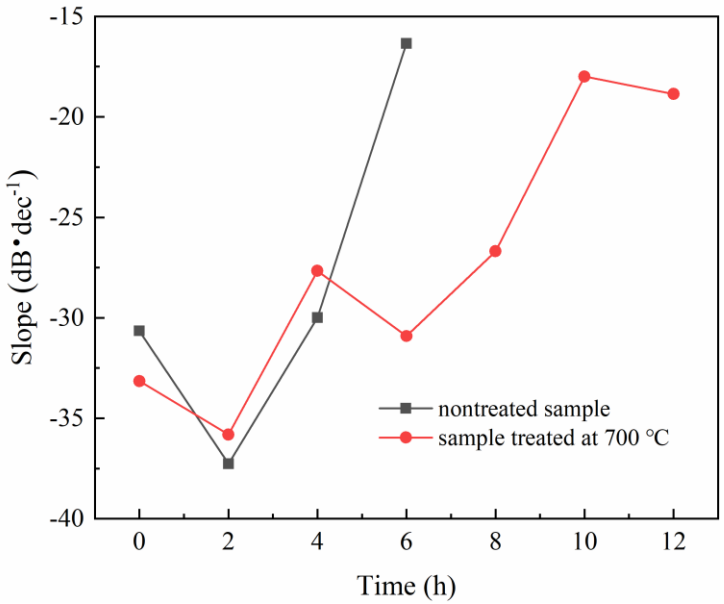

Figure 9. Slope of the power spectral density of the current noise signal of the electrochemical noise measurement of commercial annealed welded Ti-6Al-4V alloy sheets via a Rofin-DC030 pulse laser welding system before and after local rapid induction heating with different time points obtained from the slow strain rate tensile test with a strain rate of 3×10^{-7}/s in 0.1 M lithium chloride-methanol solution.

Related studies have found that the material is in a passivation state when the PSD curve slope is lower than -20 dB/dec, which is higher than -20 dB/dec and indicates that a localized corrosion process occurred on the material [32,70]. From the above results, it is clear that the occurrence time of localized corrosion of the nontreated sample is different from that of the sample treated by induction heating. Only a short length of time is required for the occurrence of localized corrosion of the nontreated sample [57-59]. After the induction heating, the occurrence time of localized corrosion is clearly delayed. There is no doubt that the relaxation of the residual stress through induction heating can effectively improve the stability of the sample surface in the corrosion medium, resulting in the later localized corrosion occurring on the sample during the slow strain rate tensile test, which effectively inhibits the stress corrosion cracking process.

3.6 Effect of residual stress on stress corrosion cracking of welded Ti-6Al-4V

For the titanium alloy, it is considered that there is a stable passivation state in the early stage of the stress corrosion cracking process under the slow strain rate tensile test, and no corrosion occurs on the sample surface at this time [45]. With the extension of the testing time under the action of tensile stress and Cl^- in the corrosion medium, the passivation state of the sample surface is continuously destroyed, which leads to the occurrence of localized corrosion [46]. A crack can be generated at the bottom of the corrosion hole, and there is a high degree of stress concentration at the bottom of the corrosion hole and the crack tip at this time. Under the influence of tensile stress and electrochemical corrosion, the crack tip dissolves and propagates rapidly until the sample finally breaks during the slow

strain rate tensile test [45,46]. The residual stress inside the material is an important factor that affects the stress corrosion cracking behavior [18-22]. In this study, the corrosion resistance of the sample has been significantly improved by adjusting the residual stress of welded Ti-6Al-4V alloy, which greatly delays the occurrence time of localized corrosion under the slow strain rate tensile test and then effectively inhibits the stress corrosion cracking process in the 0.1 M lithium chloride-methanol solution.

Comparing the nontreated sample with the sample treated at 700 ℃, the factor affecting the stress corrosion cracking sensitivity is the residual stress inside the sample. The relaxation of residual stress leads to the significant enhancement of corrosion resistance of the sample. According to Gutman's "Mechanical-Electrochemical Interactions Theory," the applied stress can significantly affect the electrochemical activity, which can be expressed through the change of the equilibrium electrochemical potential as shown in the following formula:

$$\Delta\varphi_0 = -\frac{\Delta P V_{\mathrm{m}}}{zF} \tag{7}$$

where ΔP is the stress applied to the electrode material, V_{m} is the molar volume of the electrode material, z is the charge number, and F is the Faraday constant [71]. According to the above formula, related studies have found that the tensile stress can reduce the equilibrium electrochemical potential of the sample, resulting in the increase of electrochemical activity and the decrease of corrosion resistance of the sample, and the smaller tensile stress causes the lower electrochemical activity and the higher corrosion resistance of the sample [72-74]. The tensile stress affecting the stress corrosion cracking behavior is divided into the residual stress inside the material and the working stress loaded on the material [18-22]. Therefore, this study has found that the electrochemical activity of the sample decreases and that the corrosion resistance of the sample is improved during the slow strain rate tensile test through the relaxation of residual stress, such that the occurrence time of localized corrosion is delayed. After induction heating at 700 ℃, the occurrence time of localized corrosion is delayed by 4 h compared with that of the nontreated sample; thus, the mechanical properties of the sample increase and the sensitivity of stress corrosion cracking decreases during the slow strain rate tensile test, and the stress corrosion cracking process was significantly inhibited.

4. CONCLUSIONS

In this study, the residual stress of welded Ti-6Al-4V alloy is adjusted by induction heating, and the effect of residual stress on stress corrosion cracking behavior is investigated. The residual stress in the sample decreases greatly after induction heating, and the higher induction heating temperature leads to the lower residual stress. The relaxation of residual stress improves the mechanical properties and stress corrosion cracking sensitivity of the sample under the slow strain rate tensile test. Electrochemical noise analysis shows that the sample treated by induction heating has higher corrosion resistance and a later occurrence time of localized corrosion than those of the nontreated sample during the slow strain rate tensile test. The residual stress relaxation in the welded Ti-6Al-4V alloy significantly inhibits the stress corrosion cracking process.

References

1. S. P. Trasatti and E. Sivieri, *Mater. Chem. Phys*., 83 (2004) 367.
2. M. Mihalikova, M. Hagarova, D. Jakubéczyová, J. Cervová and A. Lišková, *Int. J. Electrochem. Sci.*, 11 (2016) 4206.
3. M. O. Bodunrin, L. H. Chown, J.s W. van der Merwe, K. K. Alaneme, C. Oganbule, D. E. P. Klenam and N. P. Mphasha, *Corros. Rev.*, 38 (2020) 25.
4. Z. X. Zhang, J. K. Fan, B. Tang, H. C. Kou, J. Wang, X. Wang, S. Y. Wang, Q. J. Wang, Z. Y. Chen and J. S. Li, *J. Mater. Sci. Technol.,* 49 (2020) 56.
5. Y. K. Cao, W. D. Zhang, B. Liu, M. Song and Y. Liu, *Mater. Res. Lett.,* 8 (2020) 254.
6. L. Z. Li, S. G. Wang, W. Huang and Y. Jin, *J. Manuf. Process.,* 50 (2020) 295.
7. W. F. Xu, J. Ma, Y. X. Luo, Y. X. Fang, *T. Nonferr. Metal. Soc.,* 30 (2020) 160.
8. X. W. Yang, W. Y. Li, Y. Fu, Q. Ye, Y. X. Xu, X. R. Dong, K. W. Hu and Y. F. Zou, *J. Mater. Res. Technol.,* 8 (2019) 4797.
9. S. L. Zhang, Y. J. Ma, S. S. Huang, S. S. Youssef, M. Qi, H. Wang, J. K. Qiu, J. F. Lei and R. Yang, *J. Mater. Sci. Technol.,* 35 (2019) 1681.
10. L. D. Xiong, G. Y. Mi, C. M. Wang, G. L. Zhu, X. Xu and P. Jiang, *J. Mater. Eng. Perform.,* 28 (2019) 3349.
11. B. Kumar and S. Bag, *Opt. Laser. Eng.,* 209 (2019) 122.
12. X. Y. Song, G. L. Qian, M. Y. Zhao, Y. W. Diao, W. J. Ye and S. X. Hui, *Mater. Sci. Forum,* 944 (2019) 104.
13. G. X. Yan, A. Crivoia, Y. J. Sun, N. Maharjan, X. Song, F. Li and M. J. Tan, *J. Manuf. Process.,* 32 (2018) 763.
14. S. Josepha, T. C. Lindley, D. Dye and E. A. Saunders, *Corros. Sci.,* 134 (2018) 169.
15. D. H. Jeong, J. H. Park, S. J. Ahn, H. K. Sung, Y. N. Kwon and S. S. Kim, *Met. Mater. Int.,* 24 (2018) 101.
16. S. J. Ahn, J. H. Park, D. H. Jeong, H. K. Sung Y. N. Kwon and S. S. Kim, *Mater. Design.*, 24 (2018) 327.
17. G. Meric de Bellefon and J. C. van Duysen, *J. Nucl. Mater.,* 503 (2018) 22.
18. A. K. A. Jawwada, M. Mahdib and N. Alshabatat, *Eng. Fail. Anal.,* 105 (2019) 1229.
19. W. C. Dong, D. B. Gao and S. P. Lu, *Acta. Metall. Sin-Engl.,* 32 (2019) 618.
20. A. K. Vasudevan, K. Sadananda and P. S. Pao, *Corros. Rev.,* 37 (2019) 483.
21. W. Q. Zhang, H. C. Wu, S. Y. Wang, Y. J. Hu, K. W. Fang and X. L. Wang, *J. Mater. Eng. Perform.,* 29 (2020) 191.
22. Z. Shen, K. Arioka, S. Lozano-Pereza, *Corros. Sci.,* 132 (2018) 244.
23. S. Q. Zhang, H. Y. Zhao, F. Y. Shu, G. D. Wang, B. Liu and B. S. Xu, *Int. J. Electrochem. Sci.,* 13 (2018) 6717.
24. M. Zeidabadinejad, M. Shahidi‐Zandi, M. M. Foroughi, H. Asadollahzadeh, *Mater. Corros.,* 70 (2019) 1999.
25. Y. L. Li, C. A. Chen, Q. D., Zhong, Q. Li and Y. f. Cheng, *Surf. Rev. Lett.,* 26 (2019) 530.
26. Y. Hou, C. Aldrich, K. Lepkova and B. Kinsella, *Electrochim. Acta,* 274 (2018) 160.
27. Z. Rajabalizadeh, D. Seifzadeh, A. Habibi-Yangjeh, T. M. Gundoshmian and S. Nezamdoust, *Surf. Coat. Tech.,* 346 (2018) 29.
28. M. Leban, Ž. Bajt and A. Legat, *Electrochim. Acta,* 49 (2004) 2795.
29. J. J. Kim and S. J. Cho, *J. Mater. Sci. Lett.,* 22 (2003) 865.
30. J. G. Gonzalez-Rodriguez, M. Casales, V. M. Salinas-Bravo, M. A. Espinosa-Medina and A. Martinez-Villafane, *J. Solid. State. Eletrochem.,* 8 (2004) 290.
31. C. R. Arganis-Juarez, J. M. Malo and J. Uruchurtu, *Nucl. Eng. Des.,* 237 (2007) 2283.
32. G. Du, J. Li, W. K. Wang, C. Jiang and S. Z. Song, *Corros. Sci.,* 53 (2011) 2918.
33. C. S. Brossia, E. Gileadi and R. G. Kelly, *Corros. Sci.,* 37 (1995) 1455.

34. T. Kawai, H. Nishisara and K. Aramaki, *Corros. Sci.,* 37 (1995) 823.
35. T. Kawai, H. Nishisara and K. Aramaki, *Corros. Sci.,* 8 (1996) 225.
36. C. S. Brossia and R. G. Kelly, *Electrochim. Acta,* 41 (1996) 2579.
37. T. Kawai, H. Nishihara and K. Aramaki, *J. Electrochem. Soc.,* 143 (1996) 3866.
38. M. J. Hu and H. J. Liu, *T. Nonferr. Metal. Soc.,* 19 (2009) 324.
39. K. Q. Zhang, Z. M. Tang, S. L. Hu and P. Z. Zhang, *Nucl. Mater. Energy,* 20 (2019) 1.
40. K. S. D. Assis, C. G. C. Schuabb, M. A. Lage, M. P. P. Gonçalves, D. P. Dias and O. R. Mattos, *Corros. Sci.,* 152 (2019) 45.
41. Z. Y. Liu, W. K. Hao, W. Wu, H. Luo and X. G. Li, *Corros. Sci.,* 148 (2019) 388.
42. R. Catar and H. Altun, *Open. Chem.,* 17 (2019) 972.
43. X. Y. Zhang, R. G. Song and B. Sun, *J. Wuhan. Univ. Technol.,* 33 2018) 1198.
44. X. Q. Yue, M. F. Zhao, L. Zhang, H. J. Zhang, D. P. Li and M. X. Lu, *RSC. Adv.,* 8 (2018) 24679.
45. J. O. Yin, Y. S. Wu, J. Lu, B. F. Ding, L. Zhang and B. Cao, *Rare. Metal. Mat. Eng.,* 32 (2003) 436.
46. Y. S. Wu, Y. L. Jiang, H. Chu, Z. Y. Ding, B. F. Ding, *J. Univ. Sci. Technol. B.,* 1 (2003) 40.
47. N. S. Bharasi, A. Toppo, V. T. Paul, R. P. George and J. Philip, *J. Mater. Eng. Perform.,* 29 (2020) 2172.
48. S. X. Lin, Y. H. Huang, F. Z. Xuan and S. T. Tu, *Key. Eng. Mater.,* 795 (2019) 102.
49. Y. W. Xu, H. Y. Jing, L. Y. Xu, Y. D. Han and L. Zhao, *Constr. Build. Mater.,* 203 (2019) 642.
50. P. K. Rout and K. S. Ghosh, *Mater. Today. Proc.,* 5 (2018) 2391.
51. U. Bertocci, F. Huet and B. Jaoul, *Corrosion,* 28 (1999) 2039.
52. Ł. Lentka and J. Smulko, *Measurement,* 131 (2019) 569
53. A. Mandujano-Ruíz, J. Morales-Hernández, F. Castañeda-Saldivar, H. Herrera-Hernández and J. M. Juárez- García, *Int. J. Electrochem. Sci.,* 13 (2018) 1062.
54. C. A. Loto, *Alex. Eng. J.,* 57 (2018) 483.
55. I. Danaee and P. Nikparsa, *J. Mater. Eng. Perform.,* 28 (2019) 5088.
56. S. Q. Zhang, H. Y. Zhao, F. Y. Shu, G. D. Wang, B. Liu and B. S. Xu, *RSC. Adv.,* 8 (2018) 454.
57. Y. Liu, S. W. Tang, G. Y. Liu, Y. Sun and J. Hu, *Int. J. Electrochem. Sci.,* 11 (2016) 8530.
58. Y. Liu, S. W. Tang, G. Y. Liu, Y. Sun and J. Hu, *Int. J. Electrochem. Sci.,* 11 (2016) 10561.
59. Y. Liu, S. W. Tang, G. Y. Liu, Y. Sun and J. Hu, *Met. Mater. Int.,* 23 (2017) 488.
60. P. R. Roberge, *Corrosion,* 50 (1994) 506.
61. A. M. Nagiub, *Chinese. J. Chem.,* 24 (2006) 247.
62. C. X. Yi, X. Q. Du, Y. M. Yang, B. F. Zhu and Z. Zhang, *RSC. Adv.,* 8 (2018) 19208.
63. D. H. Xia, J. Q. Wang, Z. Wu, Z. B. Qin, L. K. Xu, W. B. Hu, Y. Behnamiand and J. L. Luo, *Sensor. Actuat. B-Chem.,* 280 (2019) 235.
64. G. Acosta, L. Veleva, J. L. Lopez, D. A. Lopez-Sauri, *T. Nonferr. Metal. Soc.,* 29 (2019) 34.
65. F. Ansari, R. Naderi and F. Rafiaei, *Pigm. Resin. Technol.,* 47 (2018) 444.
66. R. A. Cottis, A. M. Homborg and J. M. C. Mol, *Electrochim. Acta,* 202 (2016) 277.
67. C. C. Lee and F. Mansfeld, *Corros. Sci.,* 40 (1998) 959.
68. U. Bertocci, F. Huet and B. Jaoul, *Corrosion,* 28 (1999) 2039.
69. Y. F. Cheng, M. Wilmott and J. L. Luo, *Corros. Sci.,* 41 (1999) 1245.
70. J. C. Uruchurtu and J. L. Dawson, *Corrosion,* 43 (1987) 19.
71. E. M. Gutman, Mechanochemistry and Corrosion Prevention of Metals, *Science Publication,* (1989) Peking, China.
72. Y. Wang, W. Zhao, H. Ai, X. Zhou, and T. Zhang, *Corros. Sci.,* 53 (2011) 2761.
73. M. Sun, K. Xiao, C. Dong, X. Li, and P. Zhong, *Corros. Sci.,* 89 (2014) 137.
74. L. Y. Xu and Y. F. Cheng, *Corros. Sci.,* 59 (2012) 103.